Spray Coating Experiments: Setups and Methodologies
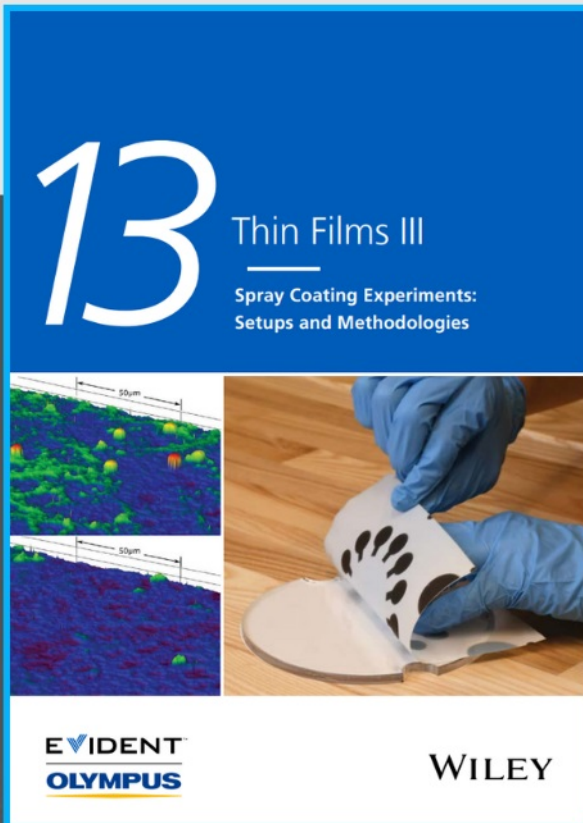

13 Thin Films III
— Spray Coating Experiments: Setups and Methodologies

The latest eBook from Advanced Optical Metrology. Download for free.

Spray Coating Experiments: Setups and Methodologies, is the third in our Thin Films eBook series. This publication provides an introduction to spray coating, three article digests from Wiley Online Library and the latest news about Evident's Image of the Year Award 2022.

Wiley in collaboration with Evident, are committed to bridging the gap between fundamental research and industrial applications in the field of optical metrology. We strive to do this by collecting and organizing existing information, making it more accessible and useful for researchers and practitioners alike.

EVIDENT OLYMPUS

WILEY

High-Yield Separation of Extracellular Vesicles Using Programmable Zwitterionic Coacervates

Carolina Paganini, Umberto Capasso Palmiero,* Sabrina Picciotto, Alessandro Molinelli, Ilaria Porello, Giorgia Adamo, Mauro Manno, Antonella Bongiovanni, and Paolo Arosio*

Programmable coacervates based on zwitterionic polymers are designed as dynamic materials for ion exchange bioseparation. These coacervates are proposed as promising materials for the purification of soft nanoparticles such as liposomes and extracellular vesicles (EVs). It is shown that the stimulus-responsiveness of the coacervates and the recruitment of desired molecules can be independently programmed by polymer design. Moreover, the polymeric coacervates can recruit and release intact liposomes, human EVs, and nanoalgosomes in high yields and separate vesicles from different types of impurities, including proteins and nucleic acids. This approach combines the speed and simplicity of precipitation methods and the programmability of chromatography with the gentleness of aqueous two-phase separation, thereby guaranteeing product stability. This material represents a promising alternative for providing a low-shear, gentle, and selective purification method for EVs.

1. Introduction

In addition to vesicle-like compartments, cells can organize functions in space and time via membraneless organelles (MLOs),[1] which are associated with liquid–liquid phase separation of proteins and nucleic acids. A remarkable feature of MLOs is their ability to selectively recruit and dynamically exchange molecules with the surrounding environment.[2–4] Recapitulating this behavior using synthetic droplets would open attractive applications in bioseparation. A key prerequisite to achieve this goal is mimicking the ability of the scaffold molecules of MLOs to encode multiple types of interactions to simultaneously control different properties of the compartments, such as stimulus-responsiveness and recruitment of client molecules.[5]

Inspired by this principle, we recently developed programmable liquid-like coacervates based on the phase separation of associative zwitterionic polymers that, in analogy with proteins commonly found in MLOs, encode multiple types of intermolecular interactions.[6] The main characteristic of this strategy is the identification of zwitterionic coacervates with three key properties: i) they reversibly form and dissolve in response to external stimuli such as temperature, pH, and ionic strength; ii) they exhibit liquid-like properties; and iii) they exhibit anti-fouling properties and preferentially exclude most molecules as well as vesicles (**Figure 1**a).[6] These baseline zwitterionic coacervates represent an ideal starting point for engineering liquid materials for biotechnological applications, particularly for the purification of biomolecules. In fact, our coacervates can be programmed to recruit target molecules by functionalizing the baseline zwitterionic polymers with specific ligands such as affinity tags or by introducing net charges, thereby attracting target compounds in the droplets based on affinity or electrostatic interactions, respectively.

In the case of recruitment by electrostatic interactions, a remarkable feature of our material is the ability to independently program the stimulus-responsiveness and recruitment of the droplets by modifying the composition and architecture of the scaffold polymer. This property makes the polymeric coacervates designed in our study significantly different from complex coacervates, in which recruitment and phase separation are both modulated by a single type of interaction, that is, attractive electrostatic forces between polyelectrolytes of opposite charges.[7,8] As a result, our material combines the advantages of a controlled partitioning with the use of a liquid and dynamic phase which responds to external stimuli.

These features are particularly attractive for processing soft products such as extracellular vesicles (EVs), whose purification currently relies on techniques such as ultracentrifugation,

C. Paganini, U. Capasso Palmiero, A. Molinelli, I. Porello, P. Arosio
Department of Chemistry and Applied Biosciences
ETH Zürich
Vladimir-Prelog-Weg 1–5/10, Zürich 8093, Switzerland
E-mail: umberto.capasso@chem.ethz.ch; paolo.arosio@chem.ethz.ch
S. Picciotto, G. Adamo, A. Bongiovanni
Institute for Research and Biomedical Innovation
National Research Council of Italy
Via Ugo la Malfa 153, Palermo 90146, Italy
S. Picciotto
Department of Biological
Chemical and Pharmaceutical Sciences and Technologies
University of Palermo
Palermo 90146, Italy
M. Manno
Institute of Biophysics
National Research Council of Italy
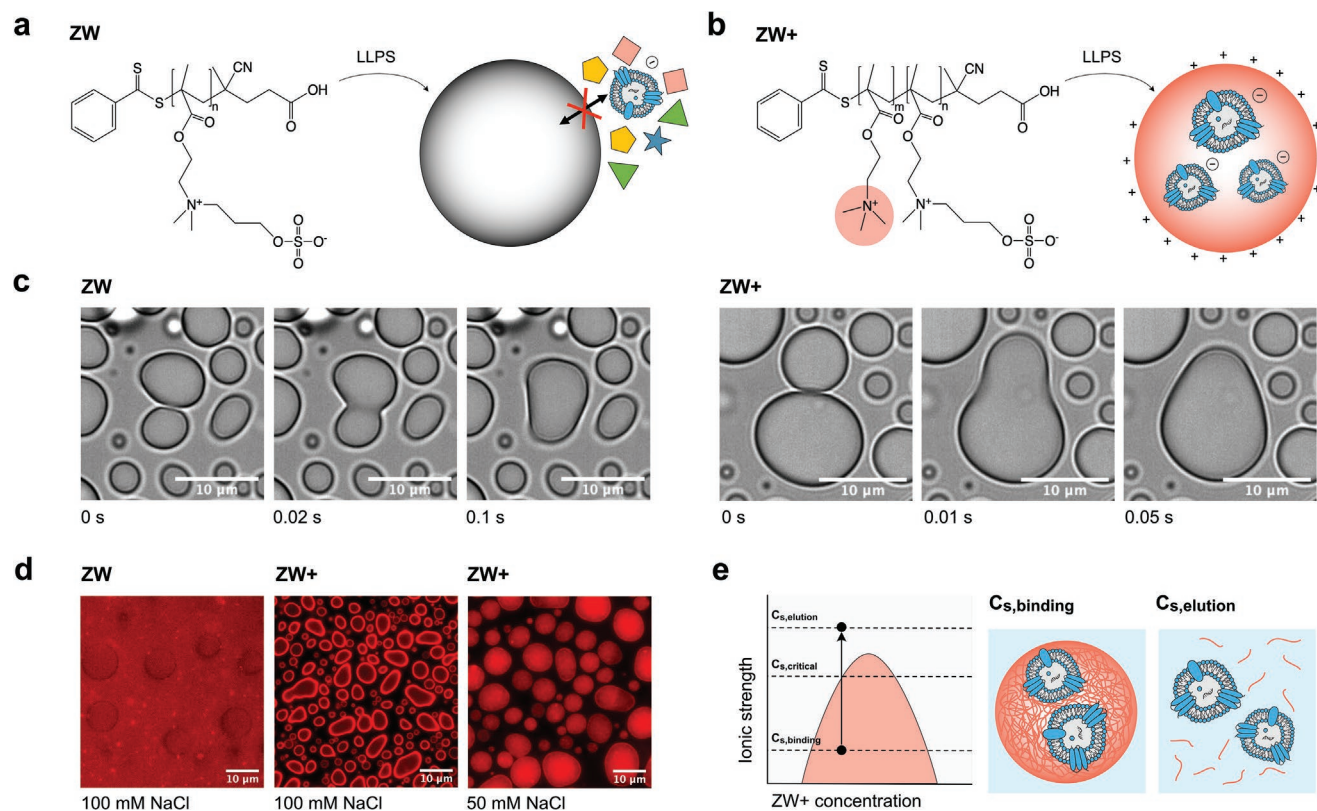Via Ugo la Malfa 153, Palermo 90146, Italy

Figure 1. Purification of extracellular vesicles (EVs) with functionalized zwitterionic coacervates. a) The baseline zwitterionic polymer (ZW) forms coacervates that largely exclude biomolecules and vesicles.[6] b) Using ZW as a starting material, we designed a polymer with both zwitterionic and unpaired positively charged monomers (ZW+), which forms coacervates capable of recruiting negatively charged vesicles via attractive electrostatic interactions. c) ZW and ZW+ coacervates behave like liquid-like material, as shown by coalescence events. d) Fluorescence microscopy images show that liposomes are excluded from ZW coacervates (left) and are recruited into ZW+ coacervates (middle and right). The location of the liposomes inside the coacervates changes with the salt concentration and therefore with the strength of the intermolecular interactions. e) Vesicles are recruited in the coacervates at low salt concentrations ($C_{s,binding}$), typically below the critical threshold required for phase separation ($C_{s,crit}$). When the salt concentration is increased above $C_{s,crit}$ ($C_{s,elution}$), coacervates dissolve and the vesicles are released in one single phase. Depending on material properties and solution conditions, $C_{s,elution}$ can be lower than $C_{s,crit}$ and vesicles can be eluted from intact coacervates.

precipitation, filtration, and chromatography.[9–16] These methods have significant issues related to low purity, high shear, and aggregation of EVs, which can alter their integrity and functionality.[13,17] In this context, our zwitterionic coacervates offer a gentler purification method.

In this study, we introduced positively charged groups in the scaffold of our zwitterionic polymers to recruit anionic species following the principle of anion exchange chromatography. These polymeric coacervates could take up and release negatively charged vesicles upon changing the salt concentration of the solution. We applied these coacervates to liposomes and extracellular vesicles obtained from HEK-293F cells and microalgae.[18,19] Moreover, we showed that our material can purify vesicles from impurities such as small molecules, proteins and DNA, demonstrating the potential use of our programmable liquid coacervates for vesicle purification from conditioned media during bioprocessing. This approach shares several key advantages with precipitation techniques, such as large purification capacity, low cost, high speed, and simple instrumentation.[20] Moreover, the gentle conditions of this method and the aqueous environment in the coacervates enable the concentration of biomolecules without affecting their stability.

2. Results

2.1. Design of Positively Charged Zwitterionic Coacervates

Starting from the baseline zwitterionic polymer (ZW) that we recently developed (Figure 1a),[6] we designed a polymer containing net positive charges (ZW+, Figure 1b). The polymer ZW+ consists of two monomers: sulfabetaine methacrylate (ZB), which is defined as the "sticker," and [2-(methacryloyloxy)ethyl]trimethylammonium (MQ), which is positively charged. ZB drives the phase separation by mediating ion-paired attractive interactions,[21] and MQ controls the uptake of negatively charged products.

First, we confirmed that the ZW+ coacervates retained the liquidity of the baseline ZW material, which is a key requirement for the purification of EVs. Initially, we used a ZW+ polymer with 20 MQ and 80 ZB monomers and observed the coalescence of the droplets formed by its liquid–liquid phase separation (LLPS) (Figure 1c).

Subsequently, we tested whether these positive coacervates could recruit negatively charged vesicles and, therefore, be used as dynamic materials for bioseparation based on ion exchange.

**ADVANCED
SCIENCE NEWS**

www.advancedsciencenews.com

NANO · MICRO

small

www.small-journal.com

To this end, we initially considered using model liposomes composed of phosphatidylserine (DOPS) and rhodamine-B-labeled phosphatidylethanolamine (RhodB-PE) at a molar ratio of 200:1 and with an average diameter of 125 nm. Given the large excess of negatively charged DOPS, the charge of the final liposomes was only minimally influenced by the presence of the fluorophores. We analyzed the uptake of the coacervates using epifluorescence microscopy. The results in Figure 1d show that the labelled liposomes did not interact with the coacervates of the unfunctionalized polymer (ZW), but were recruited into the ZW+ coacervates at low salt concentrations. We observed that the location of the liposomes in the coacervates (in both the random and block copolymers) depended on the strength of the interactions between the ZW+ polymers and the liposome membrane. Indeed, the liposomes were recruited in the bulk of the droplets when the interactions between the polymers and vesicles were strengthened (for instance, by decreasing the salt concentration or increasing the number of positive charges) (Figure 1d; Figure S2, Supporting Information).

Owing to their liquidity and recruitment capability, ZW+ coacervates can be developed as materials for EV purification. Therefore, we designed the process shown in Figure 1e. Initially, at sufficiently low salt concentrations ($C_{s,binding}$), the polymer undergoes phase separation, and the resulting droplets recruit EVs. Under these conditions, droplets enriched with EVs can be separated from the supernatant containing impurities, for instance by precipitation. The increase in salt concentration ($C_{s,elution}$) screens electrostatic interactions and allows the separation of vesicles from the dissolved droplets. Finally, the purified vesicles can be separated from the polymer via filtration or a buffer exchange step.

Notably, the programmability of zwitterionic coacervates allows one to tune $C_{s,binding}$ and $C_{s,elution}$, depending on the specificity of the system and stability of the product. For instance, in the case of EVs, although NaCl concentrations up to 1 M can be used,[14,22,23] lower ionic strengths are preferable. These salt concentrations can be easily modulated by varying the amounts of ZB and unpaired charges (MQ). In addition to controlling the uptake of negatively charged products, MQ also behaves as a "spacer." Indeed, MQ affects phase separation by changing the local concentration of ZB stickers in the polymer,[6] and increasing the repulsion between the polymers at low ionic strength.

Next, we studied the effect of unpaired positive charges on the phase separation of ZW+ to design polymers with stimulus-responsiveness in the desired salt concentration range. For this purpose, we synthesized polymers with different lengths and different numbers and distributions of unpaired positive charges (MQ). Here, the total degree of polymerization, "DP$_{tot}$," indicates the total number of monomers in the polymer. We characterized the phase separation by microscopy and measured the critical salt concentration ($C_{s,crit}$), that is, the concentration required to suppress net electrostatic attractive forces and prevent phase separation. As expected, $C_{s,crit}$ decreased with an increase in the fraction of unpaired positive charges (MQ) and therefore of the amount of electrostatic repulsion, which decreased the net attractive interactions mediated by the paired ions of the ZB monomer (**Figure 2**a). No phase separation was observed for the polymers with an MQ fraction equal to or greater than 36% (Figure 2a).

At a constant fraction of positive charges, $C_{s,crit}$ increased with increasing polymer length (Figure 2b). In agreement with Flory–Huggins theory, the critical salt concentration $C_{s,crit}$ scales with the polymer length N as per the following equation (inset Figure 2b)[24]

$$\frac{1}{\sqrt{c_{s,crit}}} = \frac{1}{\alpha}\left(\frac{1}{2} + \frac{1}{\sqrt{N}} - A\right) - \frac{B/\alpha}{T} = A' + \frac{B'}{\sqrt{N}} \tag{1}$$

Here, α is a constant, A is the temperature-independent entropic term, and B/T is the temperature-dependent enthalpic term of the non-electrostatic (residual) component of the interaction parameter χ.

$C_{s,crit}$ was only slightly affected by the distribution of the charges, as shown by the comparison between the random and block polymers (Figure 2c).

Next, we investigated the impact of the fraction and distribution of positive charges in ZW+ on the interactions between liposomes and coacervates. We incubated fluorescent liposomes with the different ZW+ polymers in a phosphate buffer containing 100 mM NaCl at pH 7.4. We characterized the partitioning by measuring the fluorescence intensity of the samples in the continuous aqueous phase. As expected, the number of liposomes recruited by the droplets increased with an increase in the fraction of positive charges (Figure 2d). Specifically, 96% of the liposomes were recruited when the fraction of positive charges was equal to or larger than 14%.

This result was independent of DP$_{tot}$, which was in the 100–600 range (Figure 2e). Combined with the data shown in Figure 2b, this result indicates that polymer length can be used as a design parameter to tune the $C_{s,crit}$ of the droplets independently of the recruitment. Therefore, the zwitterionic droplets could be adapted for specific process conditions required by the product.

Additionally, we observed that charge distribution had a significant effect on vesicle recruitment. In particular, the interactions between liposomes and droplets were strengthened when the monomers were organized into two blocks (Figure 2f). For instance, at an NaCl concentration of 150 mM, the coacervates of block and random polymers recruited 99% and 9% of the liposomes, respectively. The analysis of the distribution of condensed counterions on polymer chains with different charge patterns indicated that counterions are confined near the block charges.[25] Consequently, in the context of complex coacervation, block polymers mediate stronger attractive electrostatic interactions than random ones.[25]

Our results, which can be explained by a similar mechanism, reveal that charge patterning is an important parameter for the recruitment of droplets at the desired process operating conditions.

2.2. Separation of Liposomes with Zwitterionic Coacervates

After designing the polymers to optimize liposome recruitment, we analyzed the release of liposomes from the coacervates upon increasing the ionic strength of the solution. Based on the results described in the previous section, we selected two polymers, ZW-R1 and ZW-B1, with $C_{s,crit}$ values below 500 mM.

**ADVANCED
SCIENCE NEWS**

www.advancedsciencenews.com
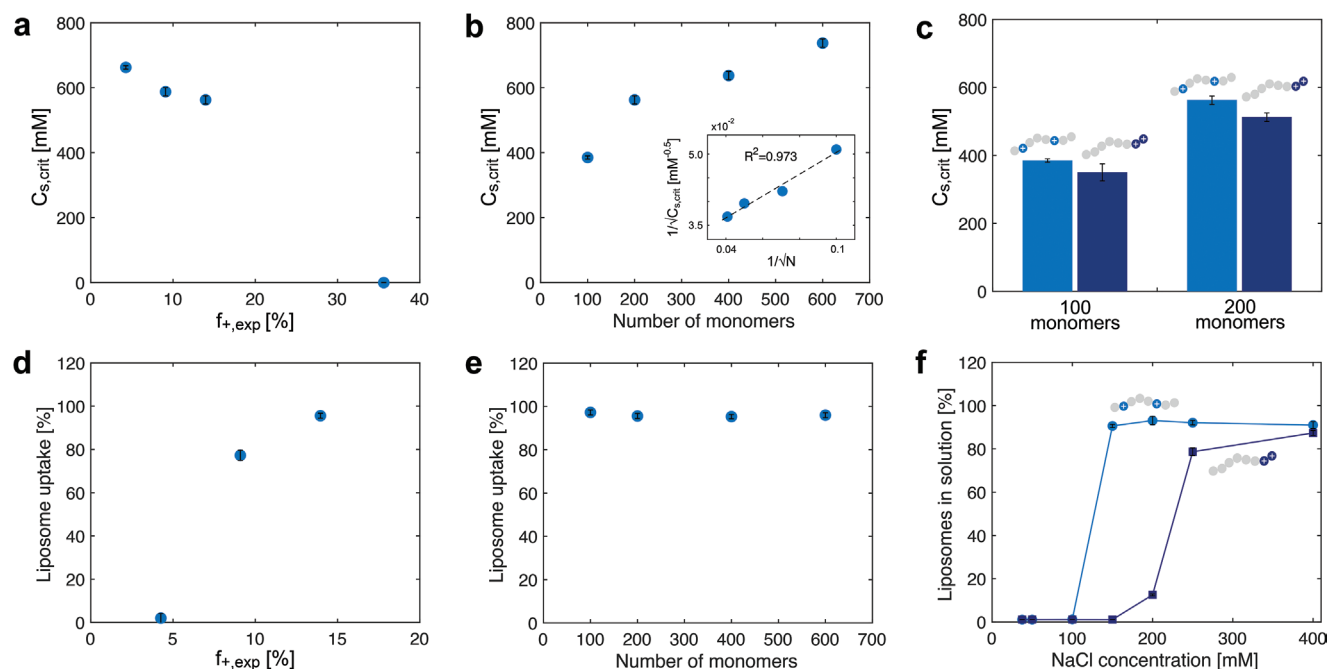
NANO · MICRO

small

www.small-journal.com

Figure 2. Independent modulation of a–c) the stimulus-responsiveness and d–f) recruitment of the ZW+ coacervates by polymer design. a) Effect of the fraction of positively charged monomers ($f_{+,exp}$) on the phase separation of ZW+ represented by the critical salt concentration ($C_{salt,crit}$). b) Effect of the length of the polymer (number of monomers, N) on the phase separation of ZW+ at a constant fraction of positively charged monomers. The inset shows predicted scaling according to the Flory-Huggins theory. c) Effect of charge distribution (random versus block) on $C_{salt,crit}$. d) Effect of the fraction of positively charged monomers on liposome recruitment. e) Effect of the length of ZW+ on liposome recruitment at a constant fraction of positively charged monomers. f) Effect of charge distribution (random vs block) on liposome recruitment. The interaction of the polymer with the liposomes increases when different monomers are organized in two blocks. All experiments were performed at constant polymer mass concentration.

The polymers were chosen to avoid NaCl concentrations at which liposome aggregation occurs. The selected polymers had similar lengths and fractions of positively charged monomers but different charge distributions. Their properties are listed in **Table 1**.

After recruiting the liposomes into the ZW+ coacervates in 100 mM NaCl, the coacervates were removed from the solution by centrifugation, and the vesicles were recovered from the polymer-rich pellet by increasing the salt concentration to 400 mM, that is, above the $C_{s,crit}$ required to dissolve the coacervates. This solution was centrifuged again to remove aggregated vesicles (**Figure 3**a).

Dynamic light scattering (DLS) measurements showed that the liposomes in the coacervates had similar size distribution before and after recruitment, demonstrating that the eluted liposomes were intact after uptake in the ZW+ coacervates (Figure 3b).

We next evaluated the separation yield by measuring the amount of liposomes recruited and released from the coacervates. For this purpose, we counted the liposomes in the

continuous phase by nanoparticle tracking analysis (NTA). The NTA measurements (Figure 3c) showed that ZW+ coacervates recruited most of the liposomes in 100 mM NaCl. Specifically, random and block polymers recruited 92 ± 1% and 96 ± 1% of liposomes, respectively. Interestingly, after increasing the salt concentration to $C_{s,elution}$ and removing the vesicle aggregates, we recovered 97 ± 10% and 78 ± 8% of the vesicles for random and block polymers, respectively. Control experiments indicated that the non-recovered fraction was formed by vesicle aggregation during centrifugation (Figure S3, Supporting Information).

Finally, we measured the binding capacity of the ZW-R1 coacervates; 0.25 mg mL⁻¹ of ZW-R1 coacervates were incubated with increasing concentrations of liposomes differing over one order of magnitude. Liposome uptake was greater than 90% at all concentrations (Figure 3d). The binding of the vesicles to the coacervates decreased their surface tension and size (Figure 3e), thereby increasing the total area available for binding. Consequently, the binding area for a fixed amount of coacervate material is not a constant parameter and depends on the number of vesicles in the solution. This is a remarkable advantage of using a liquid material over the conventional solid stationary phases used in chromatography, which can exhibit saturation effects with increasing amounts of loaded material. In contrast, the same amount of liquid coacervates can recruit vesicles with similar efficiency over a wide range of product concentrations because liquid droplets can adjust their size distribution and binding area.

Table 1. Properties of the polymers used for vesicle isolation.

	Type	DP_{ZB} [–]	DP_{MQ} [–]	DP_{tot} [–]	$f_{MQ,exp}$ [%]
ZW-R1	Random	80	20	100	9.06
ZW-B1	Block	80	20	100	13.6

2.3. Separation of Purified Extracellular Vesicles with Zwitterionic Coacervates

After demonstrating that the ZW+ coacervates can recruit and release intact liposomes in high yields and that the separation process is compatible with a wide range of product concentrations, we applied our polymeric coacervates on EVs produced from human HEK-293F cells (see characterization by microfluidic diffusion sizing,[26] NTA, and TEM in Figure S4, Supporting Information) and microalgae (see comprehensive characterization in refs. [18,27]).

We quantified the recruitment of human EVs using the ZW+ coacervates previously tested with liposomes, that is, random ZW-R1 and block ZW-B1 polymer droplets (**Figure 4**a). We quantified the recruitment of EVs by measuring their fraction remaining in the dilute phase via an ELISA assay based on tetraspanin CD81, a common EV marker.[28,29] The CD81+ particles were recruited by the ZW-R1 and ZW-B1 polymer coacervates at NaCl concentrations below 25 and 37.5 mм, respectively. These NaCl concentrations were significantly lower than the values required to recruit liposomes because the negative charge on the EV membrane was weaker than that on the liposomes. In this case, the distribution of monomers in the two

blocks did not significantly affect the salt concentration required for uptake.

The distribution of 293F-EVs inside the two different types of zwitterionic coacervates (Table 1) was investigated by imaging the coacervates using epifluorescence microscopy. EVs were labeled with a photoactivatable lipophilic dye[26,30] before incubation with ZW-R1 and ZW-B1 in 25 mм NaCl solutions and with ZW in 100 mм NaCl solutions (Figure 4b). We observed that under these conditions, EVs were concentrated mostly on the rim of the ZW-R1 and ZW-B1 coacervates. However, their locations in the droplets could be changed by tuning the strength of the interactions between the polymers and EV membrane, as demonstrated with the liposomes (Figure 1d). This mechanism is useful for controlling the local concentration of the product in the coacervates and for avoiding the potential aggregation of products at the coacervate interface due to local increase in concentration.

After identifying the conditions for EV binding, we applied the separation process previously developed for liposomes to 293F-EVs. We incubated EVs with ZW-R1 for one minute before separating the coacervates from the aqueous phase via centrifugation. The EVs were then eluted by increasing the ionic strength of the solution to 550 mм NaCl. DLS analysis of the eluates showed that the EVs recovered from the coacervates had
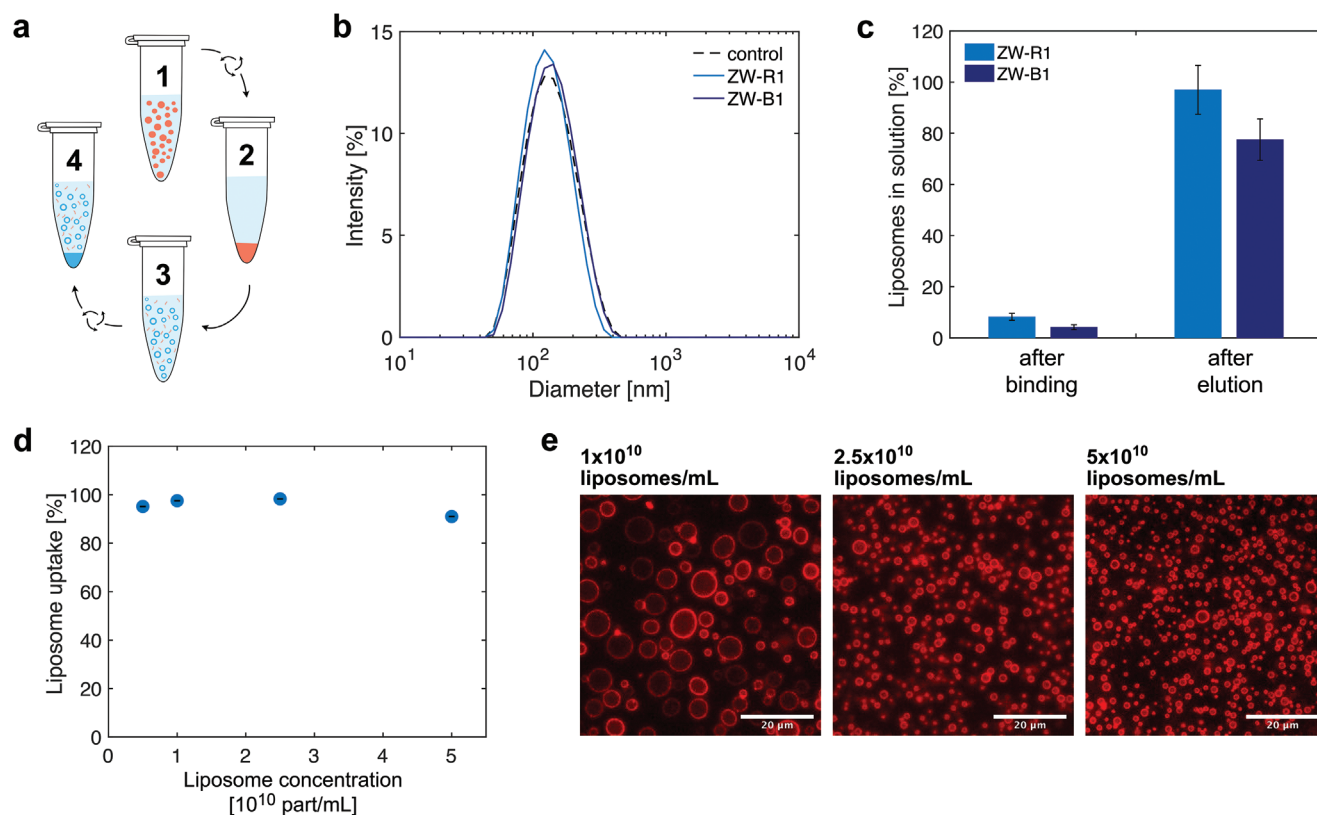

Figure 3. Liposome separation using zwitterionic coacervates. a) Schematic illustration of our process: 1) recruitment of liposomes in the ZW+ coacervates at low salt concentrations ($C_{s,binding}$), 2) separation of the ZW+ coacervates containing liposomes from the aqueous phase by centrifugation, 3) release of the liposome and dissolution of the ZW+ coacervate pellet at high salt concentration ($C_{s,elution}$), and 4) removal of the aggregates of liposomes from the final product by centrifugation. b) DLS measurements of the initial liposome samples and the liposomes recovered from the ZW+ coacervates. Most liposomes are intact after they are released from the coacervates. c) Nanoparticle tracking analysis (NTA) of the liposomes in solution after binding to the coacervates and after elution from the coacervates for random and block polymers (see Table 1). d) Coacervates can efficiently take up liposomes until a concentration of 5×10^{10} particles mL^{-1} is reached. e) Coacervate size distribution changes as a function of liposome concentration in the solution.
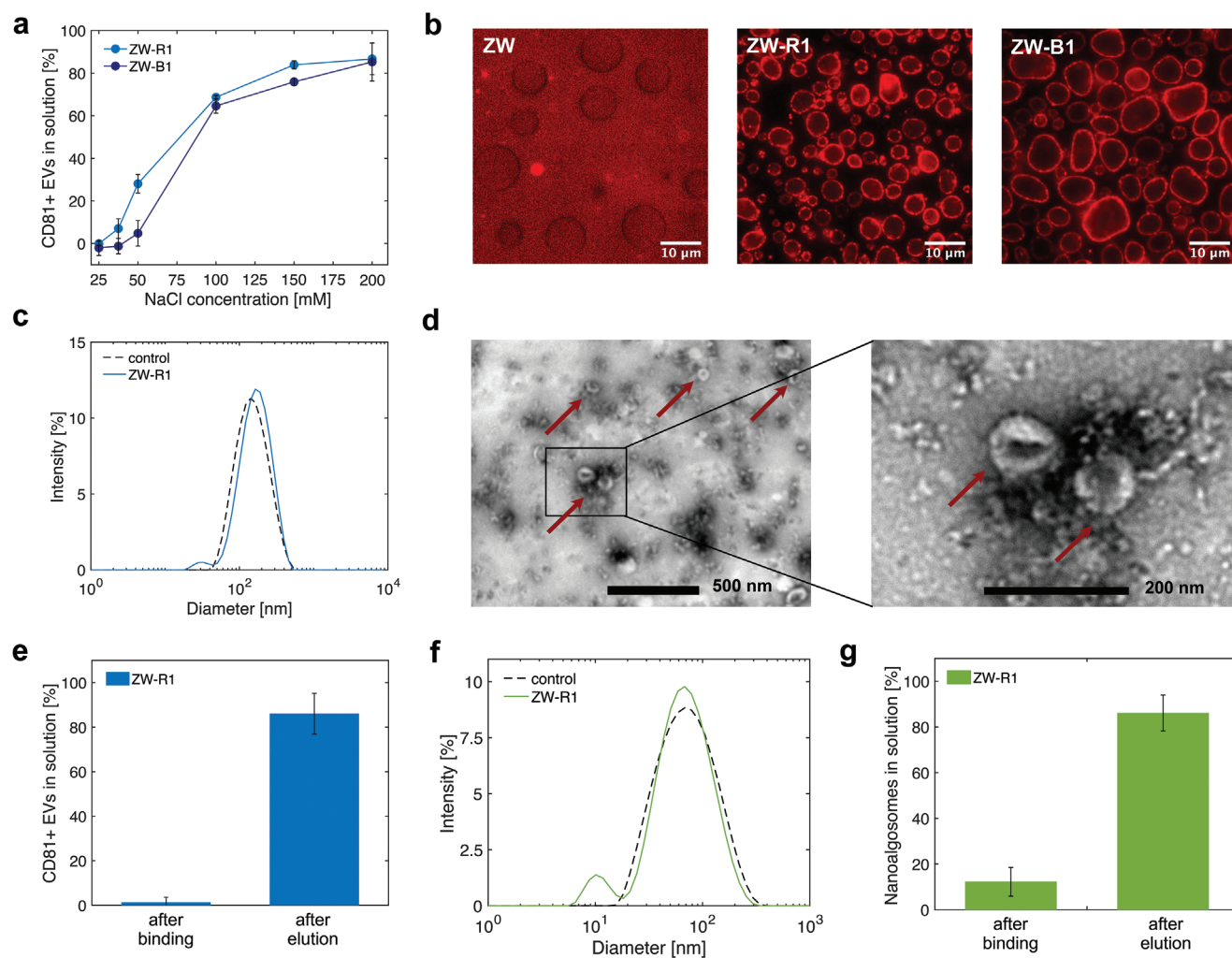
Figure 4. Separation of EVs derived from HEK 293F cells and microalgae using zwitterionic coacervates. a) ELISA measurements indicated that ZW+ coacervates recruited CD81+ EVs at different salt concentrations depending on the polymer design; ZW-R1 and ZW-B1 recruited CD81+ EVs below 25 and 37.5 mM NaCl, respectively. b) Fluorescence microscopy images showed that EVs are recruited by ZW+ coacervates and excluded by control coacervates lacking positively charged monomers (ZW). EVs also localize on the rim of the ZW-R1 and ZW-B1 droplets at 25 mM NaCl. c) DLS measurements showed that the recovered EVs have a size distribution similar to the initial EVs. d) Transmission electron microscopy (TEM) images of EVs recovered from the ZW+ coacervates. The eluate contains single cup-shaped EVs (red arrows), indicating that the process did not drastically change their morphology. e) Efficiency of the separation process assessed by ELISA measurements of the CD81 in solution. Most EVs were recruited and released from the ZW-R1 coacervates. f) DLS measurements show that the ZW+ coacervates do not affect the size distribution of the nanoalgosomes. g) NTA measurements show the uptake and release efficiency of nanoalgosomes by ZW-R1 coacervates.

a size distribution similar to that of the initial EV sample, indicating that most EVs remained intact throughout the process (Figure 4c). Moreover, TEM analysis of the eluates confirmed the presence and integrity of the isolated EVs, which exhibited the expected cup-shaped morphology (Figure 4d).

The yield of the process was measured by quantifying the amount of CD81+ particles in aqueous solutions using ELISA. We observed that most CD81+ vesicles were recruited in the ZW-R1 coacervates. Moreover, at the end of the process, we recovered 86% of the initial EVs (Figure 4e). Notably, these experiments were performed using small EVs purified by size exclusion chromatography, and different recoveries can be expected for other types of EVs.

In the case of EVs, we noticed that aggregation was mainly caused by centrifugation (Figure S5, Supporting Information).

Indeed, upon removal of the first centrifugation step, the EVs did not aggregate and nearly all EVs were recovered in the eluate (Figure S5, Supporting Information). Moreover, EV losses were significantly higher when the first centrifugation step was performed at 25 °C than at 4 °C (Figure S5, Supporting Information). Therefore, the yield can be further optimized by tuning the centrifugation settings.

To further assess the versatility of our purification approach, we tested this process on nanoalgosomes, which are EVs derived from microalgae.[18] We followed the same protocol used for 293F-EVs and used ZW-R1 coacervates. DLS measurement of the eluate confirmed that the separation of nanoalgosomes with zwitterionic coacervates did not affect their size distribution (Figure 4f). Moreover, NTA measurements showed that most nanoalgosomes were recruited by the zwitterionic

coacervates and released upon increasing the salt concentration (Figure 4g).

Under all tested conditions, the time required to complete the separation process was in the order of minutes. After polymer addition, the first binding step occurred in one minute. Our experiments confirmed that the amount of EVs recruited was unaffected by the incubation time during the interval of 1–15 min (Figure S5, Supporting Information). The second step, involving pellet dissolution and EV resuspension, was quickly performed by gently mixing the solution for a few seconds. The liquidity of the coacervates prevented the formation of EV precipitates and facilitated pellet resuspension. This property of our coacervates is more advantageous than precipitation techniques, wherein the resuspension of the product complexes is typically a challenging step.[17,31]

2.4. Purification of Extracellular Vesicles

Finally, we verified the applicability of our zwitterionic coacervates for the purification of EVs from complex solutions. As EVs and most contaminants have different charges, they interact differently with ZW+ coacervates at constant salt concentrations. Similar to anion exchange resins, the recruitment of different species in the polymer coacervates could be controlled by carefully selecting a salt concentration that minimizes the interaction of impurities.

We measured the partitioning of typical medium impurities, such as DNA and proteins, in ZW-R1 coacervates. For this purpose, HEK-293F cells were cultured in a chemically defined serum-free medium, and a small amount of clarified conditioned medium was incubated with the coacervates at different salt concentrations. We observed that approximately 82% of the DNA was recruited in ZW-R1 coacervates at 100 mM NaCl, while most proteins remained in the solution (**Figure 5**a). Proteins were also excluded at lower NaCl concentrations, whereas purified EVs were recruited in this concentration range. Proteins typically have lower charge densities than polynucleotides and are smaller in size than EVs; thus, they have fewer binding sites than the other species in the medium. By using different discrete salt concentrations, we can sequentially recruit and eliminate proteins and then separate EVs from DNA molecules.

The purification performance of ZW-R1 on nanoalgosome solutions spiked with either rhodamine B or bovine serum albumin (BSA) was tested. The NTA measurements in Figure 5b,c show that the ZW-R1 coacervates recruited 82–95% of the nanoalgosomes and released most of them upon increasing salt concentration. In contrast, only small quantities of rhodamine B and BSA (9.1 ± 1% and 4 ± 0.1%, respectively) were observed in the eluates, and they were mostly excluded from the coacervates during the binding step. This result shows the efficiency of our purification approach to isolate EVs from impurities originating from production, functionalization, or loading.

3. Discussion

Overall, our data show that our zwitterionic coacervates are promising materials for the purification of vesicles, including liposomes and human and microalgal EVs.

This method combines the advantages of various purification techniques. Similar to precipitation, liquid–liquid phase separation is a scalable method that requires simple instrumentation.[32] This process is rapid and flexible with respect to the amount of product in the solution (Figure 3e) and can adjust to fluctuations of product amounts, which is a common challenge in bioprocessing.

Similar to aqueous-two-phase systems (ATPS), our purification method is based on two liquid phases. The liquidity of the coacervates makes this approach dynamic, prevents product aggregation, and facilitates resuspension. The high water content of our zwitterionic coacervates (typically 40–50%) provides a gentle environment for bioproducts.[33] Coacervates can recruit proteins at very high concentrations, without affecting their stability.[34–36] The liquidity of the coacervates also prevents the deformation of soft vesicles, which typically occurs upon binding to solid supports. The liquid phase adapts to the vesicle shape, and thus, applies lower stress on the particle membrane.

One of the main limitations of ATPS for industrial applications is the limited control and understanding of partitioning.[33,37,38] Our method overcomes this limitation by combining the liquidity of ATPS and the programmability of chromatographic resins. Indeed, our zwitterionic coacervates can be easily programmed to recruit specific molecules from the surrounding medium and separate them from the impurities. The core principle of this strategy relies on the ability of our base polymer to preferentially exclude most molecules unless they are functionalized with charges, hydrophobic groups, or affinity tags. In this study, we functionalized the base material with unpaired charges to perform separation based on similar principles of anion exchange, one of the most common methods used at large scales to isolate biological particles during bioprocessing.[37,39–44]

Despite the increasing application of anion exchange chromatography for EVs and virus-like particles, the recovery of particles from columns is often low. Seo et al. recently reported that only 66% of loaded EVs can be recovered from a weak anion exchanger using mild elution buffers.[41] Other studies report that the recovery of EVs from a strong anion exchange resin is slightly higher than that achieved by ultracentrifugation, which is approximately 45%.[14,41,45] The reasons for these low recoveries are complex and possibly include: i) the deformation and disassembly of the vesicles on the solid supports;[46] ii) high ligand densities in the columns, the resulting binding avidity between the vesicles and resins, and harsh elution conditions for recovery;[47,48] iii) nonspecific interactions of vesicle components with the base material of the resins.[49]

The above-mentioned issues of solid resins can be avoided by using our system. As the liquid droplets adapt to the vesicle shape, the deformation of vesicles can be prevented. In addition, owing to the programmability of our material, the binding interactions and binding avidity of the vesicles can be tuned by adjusting the ionic strength of the buffer and using polymer design. Indeed, we can easily modulate the type, amount, and density of the charged monomers in the polymer. Finally, the vesicles bind to the coacervates exclusively via ionic interactions. Zwitterionic baseline polymers are often applied in antifouling coatings, as they do not interact with any molecule unless they are functionalized with specific moieties, such as the positive charges used in this work.[50–52]
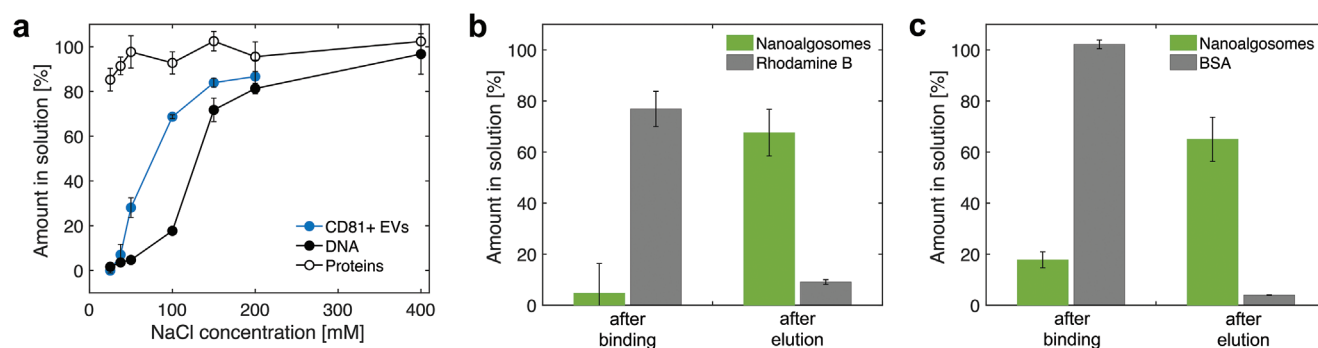
Figure 5. Separation and purification of EVs with ZW-R1 coacervates. a) Amount of protein, EVs, and DNA in solution at different salt concentrations. A low amount corresponds to a large recruitment into the coacervates. By selecting suitable salt concentrations, proteins can be removed first at low salt concentration, and EVs can be subsequently separated from DNA at higher salt concentration. Amount of nanoalgosomes in solution after binding to coacervates at low salt concentration and after elution at high salt concentration. Nanoalgosomes are recruited in ZW-R1 coacervates while b) Rhodamine B and c) BSA are preferentially excluded.

4. Conclusion

In this study, we developed programmable zwitterionic coacervates as dynamic materials for bioseparation based on anion exchange principles and demonstrated their use for the uptake and release of liposomes and EVs. Moreover, we identified key design parameters to independently control the stimulus-responsiveness and recruitment behavior of the coacervates, which can be programmed depending on specific product needs. This property of our material makes our approach very versatile. The coacervates can separate liposomes, human EVs, and nanoalgosomes from different types of impurities and release them in high yields.

Overall, this isolation approach combines the speed and simplicity of precipitation methods and the programmability of chromatography with the gentleness of a liquid-like binding phase, thereby avoiding product aggregation and degradation. This approach represents a promising alternative for low-shear, gentle, and selective purification of EVs.

5. Experimental Section

Polymer Synthesis: Polymers composed of ZB (Sulfabetaine methacrylate) and MQ ([2-(methacryloyloxy)ethyl]trimethylammonium chloride solution, 75 wt% in H_2O, Sigma-Aldrich) monomers were synthesized via reversible addition-fragmentation chain-transfer (RAFT) copolymerization using ACVA (4,4′-azobis(4-cyanovaleric acid, ≥98%, Sigma-Aldrich) as an initiator and CPA (4-cyano-4-(phenylcarbonothioylthio)pentanoic acid, ≥97%, Sigma-Aldrich) as a RAFT agent according to a previously published protocol.[6] ZB was synthesized according to a previously published method.[53] The polymers were synthesized in 20/80 v/v ethanol/3 M NaCl acetic buffer (pH 4.5) at 10 wt% total monomer concentration with a CPA to ACVA molar ratio of 3:1. The monomer-to-CPA molar ratios (that is, the degree of polymerization of a single monomer i (DP_i)) were varied, as shown in Table S1, Supporting Information. For example, in the case of ZW-R1 (the copolymer with $DP_{ZB} = 80$ and $DP_{MQ} = 20$, Table S1, Supporting Information), 846 mg of ZB, 198 mg of MQ solution, 10 mg of CPA, and 3.3 mg of ACVA were dissolved in 7.6 g of acetic buffer (pH = 4.5) and 1.5 g of ethanol and poured into a septum-sealed round bottom flask. The mixture was purged with nitrogen for 10 min and then heated to 65 °C for 24 h under constant stirring. The reaction mixture was dialyzed against 2 M NaCl for 3 days using dialysis tubing (Spectra/Por, molecular weight cut-off (MWCO) = 3.5 kDa) by frequently changing the aqueous solution. The final polymer solutions were filtered using a 0.45 μm pore size nylon membrane and stored at −20 °C. ZB/MQ block copolymers (ZWB1-2 in Table 1) were synthesized via two subsequent RAFT polymerizations following the same procedure. The first MQ-based block was produced via the RAFT polymerization of MQ in the presence of ACVA and CPA. After 24 h, 846 mg of ZB and 3.3 mg of ACVA were introduced directly into the mixture to produce the second ZB-based block. The flask was purged again with nitrogen for 10 min, and the mixture was left to react for another 24 h at 65 °C and purified according to the same procedure used for random copolymers. The copolymer concentrations were evaluated using gravimetry.

NMR Spectroscopy: The conversion (X) and MQ molar fraction ($f_{MQ,exp}$) of the copolymers (Table S1, Supporting Information) were evaluated via nuclear magnetic resonance (^1H-NMR) spectroscopy, as described in Figure S1, Supporting Information. An aliquot of each reaction mixture was collected after the completion of the reaction and purification. The samples were dried under nitrogen, dissolved in 3 M NaCl D_2O, and analyzed using a 400 MHz NMR spectrometer (Bruker).

Thermogravimetric Analysis: Thermogravimetric analysis (TGA) was performed using a Mettler Toledo TGA device to determine the polymer and salt concentrations. After purifying the polymers, approximately 1 g of dialysis water was spread on a sand-filled support to measure the salt concentration in the solution. The same procedure was followed for the polymer solutions. The actual polymer concentrations were obtained by subtracting the salt concentrations from the values measured using the polymer solution.

Critical Salt Concentration: The critical salt concentrations ($C_{s,crit}$) of the polymers were evaluated using wide-field microscopy. For this purpose, 0.25 mg mL^{-1} polymers solutions with different NaCl concentrations were incubated overnight at room temperature in a 384-well plate with a glass bottom (Brook). The wells were covered with aluminum foil to avoid evaporation and imaged after 24 h with a Ti2-U epifluorescence inverted microscope (Nikon) in the bright-field mode.

Droplet Fusion: The fusion of droplets was evaluated using a Ti2-U epifluorescence inverted microscope (Nikon) in 384-well plates. Solutions at pH 7.4 with 20 mM Na-phosphate, 100 mM NaCl, and 0.25 mg mL^{-1} of either ZB polymer (DP = 200) or a copolymer of ZB and MQ (DP = 100, $f_{ZB} = 0.8$) were prepared. The solutions were incubated at room temperature for 1 h, and the images of the wells were acquired in the brightfield mode every 5 ms to capture droplet fusion events. The surface of the wells was treated with 100 μL of 1% BSA in Millipore water for 30 min to prevent droplet wetting in the wells. The wells were washed three times with 100 μL of Millipore water before adding the polymer solutions.

Preparation of Liposomes: 1,2-dioleoyl-*sn*-glycero-3-phospho-L-serine (DOPS, Avanti Polar Lipids) and 1,2-dimyristoyl-sn-glycero-3-phosphoethanolamine-*N*-(lissamine rhodamine B sulfonyl) ammonium salt (14:0 Liss Rhod PE, Avanti Polar Lipids) were dissolved in

ADVANCED
SCIENCE NEWS
www.advancedsciencenews.com

NANO · MICRO
small
www.small-journal.com

chloroform and mixed in a DOPS/14:0 Liss Rhod PE molar ratio of 200:1. Chloroform was evaporated first with a dry nitrogen stream for 2 h and then placed under vacuum overnight. The final lipid film was hydrated with phosphate buffer saline (PBS) and gently agitated at room temperature. The lipid suspension was then extruded through a polycarbonate membrane with a pore size of 100 nm (Whatman Nucleopore Track-Etch Membrane; Cytiva) for 15 cycles. Non-fluorescent liposomes were produced in the same manner, but without the addition of 14:0 Liss Rhod PE. All lipid vesicle suspensions were stored at 4 °C.

Production of Extracellular Vesicles: 293-F cells (Gibco) were cultured at 37 °C in CD 293 medium (Gibco) supplemented with 4 mM GlutaMAX and 250 mg L^{-1} Pluronic F-68. The culture was stirred at 250 rpm and maintained at pH 7.1 and a dissolved oxygen concentration of 40% in a stirred tank bioreactor (DASGIP, Eppendorf) for 166 h. Conditioned media (450 mL) was harvested from approximately 9×10^8 cells with 92% viability and clarified by two centrifugation steps, the first at $200 \times g$ for 10 min and the second at $3000 \times g$ for 15 min. Clarified conditioned media (50 mL) was then filtered through a 0.22 µm membrane, incubated with 25 U of Pierce Universal Nuclease (Thermo Fisher Scientific) for 2.5 h at room temperature, and concentrated 100 times with an Amicon-15 centrifugal filter (50 kDa MWCO, RC membrane, Merck Millipore). The concentrated EVs (500 µL) were loaded onto a gravity flow chromatography column packed with 10 mL Sepharose CL4B resin (Cytiva). PBS was used as the running buffer to elute the EVs. Twenty fractions (500 µL each) were collected, and the ones with the highest particle number and tetraspanin CD81 concentrations measured by ELISA were pooled together, aliquoted, and stored at −80 °C.

Nanoalgosomes were produced and characterized as per a procedure described in a previous work.[27]

Microscopic Analysis of Vesicle Uptake: The uptake of fluorescent liposomes and EVs in polymer droplets was analyzed in 384-well plates (MatriPLate, Glass Bottom, Brooks) with a Ti2-U inverted microscope (Nikon) equipped with an LED light source (Omicron Laserage Laserprodukte GmbH) and a camera (Zyla sCMOS 4.2P-CL10, Andor). The filter cubes DAPI HC BP Filter set F36-500, CFP ET Filter set F46-001, EGFP ET Filter set F46-002, and Cy5 ET Filter set F46-009 (AHF Analysentechnik AG) were also used. Before adding the solutions, the wells were coated with BSA to prevent droplet wetting. Each well was incubated with 100 µL of 1% BSA in Millipore water for 30 min at room temperature and rinsed three times with Millipore water.

For liposome uptake, RhodB-DOPS liposomes of concentrations between 1×10^{10} and 5×10^{10} particles mL^{-1} were added in 100 µL solutions at pH 7.4 with 20 mM Na-phosphate, 100 mM NaCl, and 0.15 mg mL^{-1} of either ZW (DP 200), ZW-R1, or ZW-B1 (Table 1). The solutions were analyzed after incubating the samples for at least 1 h at room temperature.

For EV uptake, EVs were first labelled with photoactivatable silicon rhodamine, as previously described.[26] A 20 µM dye was added to a stock solution containing 9×10^{10} particles mL^{-1} of HEK-293F EVs, and the resultant solution was immediately photoactivated with UV light for 2 min. EVs were then introduced at 1×10^9 particles mL^{-1} in the corresponding samples containing 0.15 mg mL^{-1} of ZW, ZW-R1, or ZW-B1 (Table 1). Images were acquired after incubating the EVs for at least 1 h at room temperature.

ELISA: Quantification of CD81 in the samples was performed using 96-well plates (TPP). Samples (50 µL per well) were diluted to obtain 100 µL solutions containing 1 M NaCl and 20 mM Na-phosphate. The pH of this solution was kept at 7.4, and the resultant solution was incubated overnight at 4 °C. The plate was then washed with high-salt buffer (20 mM Na-phosphate, 1 M NaCl, pH 7.4) and PBS and blocked with 1% BSA in PBS for 1 h at room temperature. Next, the plate was incubated with the anti-human CD81 antibody 5A6 (1:500 dilution in blocking buffer; Santa Cruz Biotechnology) for 2 h at room temperature. After extensive washing, the plate was incubated with the secondary anti-mouse HRP-conjugated antibody (1:2000 dilution in blocking buffer; m-IgGκ BP-HRP; Santa Cruz Biotechnology) for 1 h at room temperature. Finally, the plate was washed and incubated with TMB ELISA Substrate (highest sensitivity, Abcam) for 15 min at room temperature. Subsequently, 450 nm STOP Solution was added to the TMB substrate (Abcam), and the absorbance of the resultant solution was measured at 450 nm using a Clariostar Plus microplate reader (BMG Labtech).

Nanoparticle Tracking Analysis (NTA) Measurements: NTA measurements of liposomes and nanoalgosomes were performed using a ZetaView instrument equipped with a CMOS camera and a 405 nm laser (Particle Metrix). The chamber was calibrated daily with polystyrene nanoparticle standards, as per the manufacturer's recommendations. Samples were diluted in a high-salt buffer (20 mM Na-phosphate, 400 mM, or 1 M NaCl, pH 7.4) to a particle concentration of 10^7–10^9 particles mL^{-1} and injected into the sample chamber using a 1 mL syringe until the chamber was filled. Video acquisition was performed for all samples at 11 positions with 80% scattering intensity and 100 shutter in the light scattering mode, with a trace length of 15 frames and a frame rate of 30 s^{-1}. Data were analyzed using the ZetaView analysis software (ZetaView 8.04.02 SP2).

Quantitative Analysis of the Uptake and Release of Liposomes, EVs, and Nanoalgosomes: For these experiments, solutions were prepared in 1.5 mL microcentrifuge tubes, and the polymer was subsequently added.

The uptake of liposomes was measured at different salt concentrations. For this purpose, 300 µL solutions (pH 7.4) containing 0.25 mg mL^{-1} ZW-R1 or ZW-B1 (Table 1), 3×10^9 particles mL^{-1} liposomes, 20 mM Na-phosphate, and different NaCl concentrations (37.5, 50, 100, 150, 200, 250, and 400 mM) were prepared. These solutions were briefly vortexed and incubated for 15 min at room temperature. The tubes were then centrifuged at $10\,000 \times g$ for 15 min at 25 °C. The supernatant (270 µL) was removed, and its fluorescence intensity was measured using a ClarioStar Plus microplate reader (BMG Labtech) at excitation and emission wavelengths of 550 and 605 nm, respectively. Measurements were performed in triplicate.

The liposome uptake in ZW-R1 coacervates at different liposome concentrations (in the range of 5×10^9–1×10^{11} particles mL^{-1}) was analyzed in a similar manner at a constant NaCl concentration of 100 mM. Solutions were centrifuged at $3000 \times g$ for 15 min at 25 °C.

To measure the recovery of liposomes from the coacervates, solutions (300 µL, pH 7.4) containing 20 mM Na-phosphate, 100 mM NaCl, 0.25 mg mL^{-1} ZW-R1 or ZW-B1, and 1.3×10^{10} particles mL^{-1} of non-fluorescent DOPS liposomes were prepared. After polymer addition, these solutions were incubated for 1 min at room temperature and then centrifuged at $3000 \times g$ for 5 min at 4 °C. Then, the supernatant (270 µL) was removed and replaced with high-salt buffer (270 µL) to obtain a solution (pH 7.4) containing 20 mM Na-phosphate and 400 mM NaCl. The polymer pellet was resuspended by gentle pipetting and vortexed for several seconds. The resuspended sample was centrifuged at $3000 \times g$ for 15 min at 25 °C, and the supernatant (270 µL) was removed. All supernatants recovered during the process were analyzed using NTA to quantify the amounts of unbound and eluted liposomes. Measurements were performed in triplicate.

The uptake of HEK-293F EVs was measured by preparing solutions (150 µL, pH 7.4) containing 0.25 mg mL^{-1} ZW-R1 or ZW-B1, 5×10^9 particles mL^{-1} HEK-293F EVs, 20 mM Na-phosphate, and different NaCl concentrations (25, 37.5, 50, 100, 150, and 200 mM). Samples were mixed by gentle vortexing and incubated for 15 min at room temperature. Then, the tubes were centrifuged at $3000 \times g$ for 15 min at 25 °C. The supernatant (125 µL) was removed and analyzed using ELISA. Measurements were performed in duplicate for two independent samples.

The recovery of HEK-293F EVs was measured by following the same procedure used for liposomes. The ZW-R1 polymer (0.25 mg mL^{-1}) was introduced in solutions (300 µL, pH 7.4) containing 20 mM Na-phosphate, 12.5 mM NaCl, and 5×10^9 particles mL^{-1} of HEK-293F EVs. After adding the polymer, the solutions were incubated for 1 min at room temperature and centrifuged at $370 \times g$ for 21 min at 4 °C. After removing the supernatant, pellets of ZW-R1 were resuspended in high-salt buffers containing 550 mM NaCl. The second centrifugation was then performed at $3000 \times g$ for 15 min at 25 °C. All collected supernatants were analyzed using ELISA. The measurements were

2204736 (9 of 11)

ADVANCED
SCIENCE NEWS
www.advancedsciencenews.com

NANO · MICRO
small
www.small-journal.com

performed in duplicate for three independent samples. For transmission electron microscopy (TEM), the same protocol was followed for 1×10^{10} particles mL^{-1} of HEK-293F EVs, and the pellets were resuspended in high salt buffer (40 µL).

The recovery of the nanoalgosomes was measured by following the same procedure used for HEK-293F EVs. The number of particles in the supernatants was determined using NTA. Measurements were performed in duplicate for two independent samples.

To measure the uptake of medium impurities in ZW-R1 coacervates, solutions (300 µL, pH 7.4) containing clarified conditioned medium (15 µL) from HEK-293F cultures, 0.25 mg mL^{-1} ZW-R1, 20 mM Na-phosphate, and different NaCl concentrations (25, 37.5, 50, 100, 150, 200, and 400 mM) were prepared. Samples were mixed by gentle vortexing and incubated for 15 min at room temperature. Subsequently, the tubes were centrifuged at $3000 \times g$ for 15 min at 25 °C. The supernatants (270 µL) were removed and analyzed using the QuantIT dsDNA Assay Kit (highest sensitivity, Thermo Fisher Scientific) and Micro BCA Protein Assay Kit (Thermo Fisher Scientific) in duplicate.

Finally, to test the purification of nanoalgosomes from Rhodamine B and BSA, solution (300 µL, pH 7.4) were prepared using 20 mM Na-phosphate, 12.5 mM NaCl, 0.25 mg mL^{-1} ZW-R1, 5×10^9 particles mL^{-1} of nanoalgosomes, and 1.5 µM Rhodamine B or 1.5 µM BSA (Sigma-Aldrich) labelled with Rhodamine B. The samples were incubated for 1 min at room temperature and centrifuged at $3000 \times g$ for 5 min at 4 °C. After removing the supernatant, the samples were resuspended in high-salt buffer with 550 mM NaCl and 20 mM Na-phosphate at pH 7.4. The second centrifugation was then performed at $3000 \times g$ for 15 min at 25 °C. The number of particles in the supernatants was measured in duplicates by NTA, and their fluorescence intensities were analyzed in triplicate at excitation and emission wavelengths of 550 and 605 nm, respectively, using a Clariostar Plus microplate reader (BMG Labtech).

Dynamic Light Scattering (DLS) Measurements: The size distributions of the non-fluorescent liposomes, HEK-293F EVs, and the nanoalgosomes were measured using a Zetasizer Nano ZSP DLS system (Malvern) in backscattering mode at 173° and 20 °C.

Transmission Electron Microscopy: Five microliters of sample was placed on glow discharged (negatively at 25 mA for 30 s in an Emitech K100X glow discharge system, Quorum Technologies Ltd.) carbon-coated grids (Plano GmbH) and allowed to adsorb for 60 s. Subsequently, the excess liquid was drained with a filter paper, and the samples were subjected to negative staining with 2% uranyl acetate (w/v) by two successive incubations of 1 and 15 s. The grids were air-dried and imaged using a JEM-1400Flash electron microscope (JOEL) in the bright-field mode operated at 100 kV.

Fluorescence-Based Microfluidic Diffusion Sizing (fluoMDS) Measurements: FluoMDS analysis was performed as described in a previous study.[26] For lipid staining, HEK-293F EVs were mixed with 20 µM photoactivatable silicon rhodamine[30] and photoactivated with UV light for 2 min. For labeling the tetraspanins, HEK-293F EVs were blocked for 1 h at room temperature with 0.1% BSA in PBS and incubated with APC-conjugated anti-CD81 antibodies (1D6, 1:500 dilution in blocking buffer, Invitrogen) and PE-conjugated anti-CD63 antibodies (H5C6, 1:500 dilution in blocking buffer, Invitrogen). All samples had a final particle concentration of 1.5×10^{11} particles mL^{-1}. Five microliters of sample were then loaded in the fluoMDS device, which was run at 60 µL h^{-1} using blocking buffer as the running buffer. After image acquisition with a Ti2-U inverted microscope (Nikon), the diffusion profiles were fitted, and the average particle sizes were computed as previously reported.[26]

EV Track: All relevant data from these experiments were submitted to the EV-TRACK knowledgebase (EV-TRACK ID: EV220295).[54]

Statistical Analysis: The number of particles in the solution [%] was referred to as the control sample without the polymer. All data were presented as mean ± standard deviation.

Supporting Information

Supporting Information is available from the Wiley Online Library or from the author.

Conflict of Interest

The authors declare no conflict of interest.

Data Availability Statement

The data that support the findings of this study are available from the corresponding author upon reasonable request.

[1] S. F. Banani, H. O. Lee, A. A. Hyman, M. K. Rosen, *Nat. Rev. Mol. Cell Biol.* **2017**, *18*, 285.

[2] B. G. O'Flynn, T. Mittag, *Curr. Opin. Cell Biol.* **2021**, *69*, 70.

[3] S. Boeynaems, S. Alberti, N. L. Fawzi, T. Mittag, M. Polymenidou, F. Rousseau, J. Schymkowitz, J. Shorter, B. Wolozin, L. Van Den Bosch, P. Tompa, M. Fuxreiter, *Trends Cell Biol.* **2018**, *28*, 420.

[4] E. Gomes, J. Shorter, *J. Biol. Chem.* **2019**, *294*, 7115.

[5] H. Zhao, E. Ibarboure, V. Ibrahimova, Y. Xiao, E. Garanger, S. Lecommandoux, *Adv. Sci.* **2021**, *8*, 2102508.

[6] U. Capasso Palmiero, C. Paganini, M. R. G. Kopp, M. Linsenmeier, A. M. Küffner, P. Arosio, *Adv. Mater.* **2022**, *34*, 2104837.

[7] A. M. Rumyantsev, N. E. Jackson, J. J. De Pablo, *Annu. Rev. Condens. Matter Phys.* **2021**, *12*, 155.

[8] C. E. Sing, S. L. Perry, *Soft Matter* **2020**, *16*, 2885.

[9] C. Paganini, U. Capasso Palmiero, G. Pocsfalvi, N. Touzet, A. Bongiovanni, P. Arosio, *Biotechnol. J.* **2019**, *14*, 1800528.

[10] J. Chen, P. Li, T. Zhang, Z. Xu, X. Huang, R. Wang, L. Du, *Front. Bioeng. Biotechnol.* **2022**, *9*, 811971.

[11] T. Liangsupree, E. Multia, M. L. Riekkola, *J. Chromatogr. A* **2021**, *1636*, 461773.

[12] I. K. Herrmann, M. J. A. Wood, G. Fuhrmann, *Nat. Nanotechnol.* **2021**, *16*, 748.

[13] C. Gardiner, D. Di Vizio, S. Sahoo, C. Théry, K. W. Witwer, M. Wauben, A. F. Hill, *J. Extracell. Vesicles* **2016**, *5*, 32945.

[14] N. Heath, L. Grant, T. M. De Oliveira, R. Rowlinson, X. Osteikoetxea, N. Dekker, R. Overman, *Sci. Rep.* **2018**, *8*, 5730.

[15] I. L. Colao, R. Corteling, D. Bracewell, I. Wall, *Trends Mol. Med.* **2018**, *24*, 242.

[16] B. Barnes, T. Caws, S. Thomas, A. P. Shephard, R. Corteling, P. Hole, D. G. Bracewell, *J. Chromatogr. A* **2022**, *1670*, 462987.

[17] M. Y. Konoshenko, E. A. Lekchnov, A. V. Vlassov, P. P. Laktionov, *Biomed. Res. Int.* **2018**, 8545347.

[18] G. Adamo, M. E. Barone, D. Fierli, A. Aranyos, D. P. Romancino, S. Picciotto, M. Gai, R. Carrotta, S. Morsbach, S. Raccosta, C. Stanly, C. Paganini, A. Cusimano, V. Martorana, R. Noto, F. Librizzi, L. Randazzo, R. Parkes, E. Rao, A. Paterna, P. Santonicola, A. Kisslinger, V. Kralj-igliˇ, U. C. Palmiero, L. Corcuera, E. Di Schiavi, G. L. Liguori, K. Landfester, P. Arosio, G. Pocsfalvi, et al., *J. Extracell. Vesicles* **2021**, *10*, e12081.

[19] S. Picciotto, M. E. Barone, D. Fierli, A. Aranyos, G. Adamo, D. Božič, D. P. Romancino, C. Stanly, R. Parkes, S. Morsbach, S. Raccosta, C. Paganini, A. Cusimano, V. Martorana, R. Noto, R. Carrotta, F. Librizzi, U. Capasso Palmiero, P. Santonicola, A. Iglič, M. Gai, L. Corcuera, A. Kisslinger, E. Di Schiavi, K. Landfester, G. L. Liguori, V. Kralj-Iglič, P. Arosio, G. Pocsfalvi, M. Manno, et al., *Biomater. Sci.* **2021**, *9*, 2917.

[20] Y. Xu, M. Mazzawi, K. Chen, L. Sun, P. L. Dubin, *Biomacromolecules* **2011**, *12*, 1512.

[21] J. D. Delgado, J. B. Schlenoff, *Macromolecules* **2017**, *50*, 4454.

[22] R. Upadhya, L. N. Madhu, S. Attaluri, D. L. G. Gitaí, M. R. Pinson, M. Kodali, G. Shetty, G. Zanirati, S. Kumar, B. Shuai, S. T. Weintraub, A. K. Shetty, *J. Extracell. Vesicles* **2020**, *9*, 1809064.

[23] V. Luga, L. Zhang, A. M. Viloria-Petit, A. A. Ogunjimi, M. R. Inanlou, E. Chiu, M. Buchanan, A. N. Hosein, M. Basik, J. L. Wrana, *Cell* **2012**, *151*, 1542.

[24] T. Lu, K. K. Nakashima, E. Spruijt, *J. Phys. Chem. B* **2021**, *125*, 3080.

[25] L. W. Chang, T. K. Lytle, M. Radhakrishna, J. J. Madinya, J. Vélez, C. E. Sing, S. L. Perry, *Nat. Commun.* **2017**, *8*, 1273.

[26] C. Paganini, B. Hettich, M. R. G. Kopp, A. Eördögh, U. Capasso Palmiero, G. Adamo, N. Touzet, M. Manno, A. Bongiovanni, P. Rivera-Fuentes, J. C. Leroux, P. Arosio, *Adv. Healthcare Mater.* **2021**, *11*, 2100021.

[27] A. Paterna, E. Rao, G. Adamo, S. Raccosta, S. Picciotto, D. Romancino, R. Noto, N. Touzet, A. Bongiovanni, M. Manno, *Front. Bioeng. Biotechnol.* **2022**, *10*, 836747.

[28] J. Kowal, G. Arras, M. Colombo, M. Jouve, J. P. Morath, B. Primdal-Bengtson, F. Dingli, D. Loew, M. Tkach, C. Théry, *Proc. Natl. Acad. Sci. U. S. A.* **2016**, *113*, E968.

[29] D. K. Jeppesen, A. M. Fenix, J. L. Franklin, J. N. Higginbotham, Q. Zhang, L. J. Zimmerman, D. C. Liebler, J. Ping, Q. Liu, R. Evans, W. H. Fissell, J. G. Patton, L. H. Rome, D. T. Burnette, R. J. Coffey, *Cell* **2019**, *177*, 428.

[30] A. Eördögh, C. Paganini, D. Pinotsi, P. Arosio, P. Rivera-Fuentes, *ACS Chem. Biol.* **2020**, *15*, 2597.

[31] N. Hammerschmidt, S. Hobiger, A. Jungbauer, *Process Biochem.* **2016**, *51*, 325.

[32] M. Martinez, M. Spitali, E. L. Norrant, D. G. Bracewell, *Trends Biotechnol.* **2019**, *37*, 237.

[33] M. Iqbal, Y. Tao, S. Xie, Y. Zhu, D. Chen, X. Wang, L. Huang, D. Peng, A. Sattar, M. A. B. Shabbir, H. I. Hussain, S. Ahmed, Z. Yuan, *Biol. Proced. Online* **2016**, *18*, 18.

[34] W. C. Blocher McTigue, S. L. Perry, *Soft Matter* **2019**, *15*, 3089.

[35] L. Zhou, H. Shi, Z. Li, C. He, *Macromol. Rapid Commun.* **2020**, *41*, 1.

[36] W. C. Blocher McTigue, S. L. Perry, *Small* **2020**, *16*, 1907671.

[37] P. Nestola, C. Peixoto, R. R. J. S. Silva, P. M. Alves, J. P. B. Mota, M. J. T. Carrondo, *Biotechnol. Bioeng.* **2015**, *112*, 843.

[38] H. O. Johansson, J. Persson, F. Tjerneld, *Biotechnol. Bioeng.* **1999**, *66*, 247.

[39] S. B. Carvalho, C. Peixoto, M. J. Manuel, R. J. Ricardo, *Biotechnol. Bioeng.* **2021**, *118*, 2845.

[40] M. G. Moleirinho, R. J. S. Silva, P. M. Alves, M. J. T. Carrondo, C. Peixoto, *Expert Opin. Biol. Ther.* **2020**, *20*, 451.

[41] N. Seo, J. Nakamura, T. Kaneda, H. Tateno, A. Shimoda, T. Ichiki, K. Furukawa, J. Hirabayashi, K. Akiyoshi, H. Shiku, *J. Extracell. Vesicles* **2022**, *11*, e12205.

[42] S. Fedosyuk, T. Merritt, M. P. Peralta-Alvarez, S. J. Morris, A. Lam, N. Laroudie, A. Kangokar, D. Wright, G. M. Warimwe, P. Angell-Manning, A. J. Ritchie, S. C. Gilbert, A. Xenopoulos, A. Boumlic, A. D. Douglas, *Vaccine* **2019**, *37*, 6951.

[43] M. Kosanovic, B. Milutinovic, S. Goc, N. Mitic, M. Jankovic, *BioTechniques* **2017**, *63*, 65.

[44] J. Ruscic, C. Perry, T. Mukhopadhyay, Y. Takeuchi, D. G. Bracewell, *Mol. Ther. Methods Clin. Dev.* **2019**, *15*, 52.

[45] D.-K. Kim, H. Nishida, S. Y. An, A. K. Shetty, T. J. Bartosh, D. J. Prockop, *Proc. Natl. Acad. Sci. U. S. A.* **2016**, *113*, 170.

[46] M. Yu, Y. Li, S. Zhang, X. Li, Y. Yang, Y. Chen, G. Ma, Z. Su, *J. Chromatogr. A* **2014**, *1331*, 69.

[47] T. Vicente, R. Fáber, P. M. Alves, M. J. T. Carrondo, J. P. B. Mota, *Biotechnol. Bioeng.* **2011**, *108*, 1347.

[48] H. Park, T. N. Sut, B. K. Yoon, V. P. Zhdanov, N. J. Cho, J. A. Jackman, *J. Phys. Chem. Lett.* **2021**, *12*, 6722.

[49] E. Lerer, Z. Oren, Y. Kafri, Y. Adar, E. Toister, L. Cherry, E. Lupu, A. Monash, R. Levy, E. Dor, E. Epstein, L. Levin, M. Girshengorn, N. Natan, R. Zichel, A. Makovitzki, *BioTech* **2021**, *10*, 22.

[50] J. Ladd, Z. Zhang, S. Chen, J. C. Hower, S. Jiang, *Biomacromolecules* **2008**, *9*, 1357.

[51] L. D. Blackman, P. A. Gunatillake, P. Cass, K. E. S. Locock, *Chem. Soc. Rev.* **2019**, *48*, 757.

[52] N. Y. Kostina, S. Sharifi, A. De Los Santos Pereira, J. Michálek, D. W. Grijpma, C. Rodriguez-Emmenegger, *J. Mater. Chem. B* **2013**, *1*, 5644.

[53] M. Sponchioni, P. Rodrigues Bassam, D. Moscatelli, P. Arosio, U. C. Palmiero, *Nanoscale* **2019**, *11*, 16582.

[54] J. van Deun, P. Mestdagh, P. Agostinis, Ö. Akay, S. Anand, J. Anckaert, Z. A. Martinez, T. Baetens, E. Beghein, L. Bertier, G. Berx, J. Boere, S. Boukouris, M. Bremer, D. Buschmann, J. B. Byrd, C. Casert, L. Cheng, A. Cmoch, D. Daveloose, E. De Smedt, S. Demirsoy, V. Depoorter, B. Dhondt, T. A. P. Driedonks, A. Dudek, A. Elsharawy, I. Floris, A. D. Foers, K. Gärtner, et al., *Nat. Methods* **2017**, *14*, 228.